



MataMorph 2: A new experimental UAV with twist-morphing wings and camber-morphing tail stabilizers

Adam E. Schlup¹, Tommy L. MacLennan¹, Cristobal Barajas¹, Bianca L. Talebian¹, Gregory C. Thatcher¹, Richard B. Flores¹, Justin D. Perez-Norwood¹, Christian L. Torres¹, Kebron B. Kibret¹, Edgar E. Guzman¹
and

Dr. Peter L. Bishay²

California State University, Northridge, Northridge, CA, 91330, United States

Morphing technology aims to improve both aerodynamic and power efficiency of aircrafts by eliminating traditional control surfaces and implementing uniform wings with seamless shape-changing ability. A lot of research has focused on proposing new designs for morphing wings, without implementation in a flying aircraft. Only few papers reported the design and flight-testing of unmanned aerial vehicles (UAVs) with morphing surfaces. Most of such designs focused only on wings, while the tail stabilizers are conventionally designed. This paper presents Matamorph-2 (XM-2), a fully morphing UAV with twisting wings and variable-camber tail stabilizers. XM-2 can perform all required maneuvers without any discrete control surfaces. The wings feature balsa wood structure, wing-root and wing-tip laminated composite skin sections and a twisting section made of polyurethane foam covered by a smooth flexible skin. With a $\pm 15^\circ$ range of twisting motion, XM-2 wings do not need flaps, slats or ailerons to control lift and roll generated by the UAV. Each tail stabilizer consists of a rigid leading-edge section connected to a camber-morphing corrugated trailing edge section. The tail rib design is a new version of the “FishBAC” rib with flexible carbon fiber composite ribbons running through the corrugated section to actuate the rib. The corrugated trailing edge section is 3D printed of flexible PCTPE plastic that balances between rigidity and flexibility. When compared to much-smaller traditional control surfaces, these large camber-morphing surfaces provide more power and control in a much smaller dimensional envelope. The paper presents the detailed design of all components, simulations, assembly and mechanical testing. XM-2 aims to prove that flight is possible without drag-inducing discrete control surfaces, and encourages further discovery of fully morphing UAVs.

I. Introduction

Conventional aircraft utilize discrete hinged control surfaces, such as flaps, ailerons, elevators, and rudders to modify aerodynamic performance and maneuver during flight. Although conventional flight control surfaces are effective in controlling the aircraft, they introduce discontinuities in the aerodynamic profile. The gaps and discontinuities disturb the flow of air over the aircraft, creating vortices that induce drag. Power efficiency is heavily tied to drag, and a small change in aircraft design to minimize drag can have a significant impact on the overall aircraft efficiency. Accordingly, addressing drag issues caused by conventional control surfaces using aircraft morphing wing technology is vital to improving aircraft efficiency. Wing morphing is not a new concept. It has been explored since the inception of flight. In fact, the Wright Flyer utilized twisting wing morphing to control the pitch and roll of the plane. Moreover, nature is filled with creatures whose wing shape changes dynamically to suit different flight conditions and still remain lightweight. Morphing research seeks to replicate nature’s effectiveness. However, achieving aerodynamic efficiency while maintaining low weight has been a challenge due to limitations of materials and the necessary mechanical structures to control the morphing¹⁻⁶. New technologies and materials have reinvigorated the development and feasibility of morphing wing technology⁷⁻⁹.

Morphing geometry changes can be classified into two primary categories, out-of-plane, and in-plane morphing³. In-plane morphing retains the wing within the plane of the airfoil cross section, and includes span, sweep, or oblique wing morphing. Out-of-plane morphing changes the geometry of the airfoil cross section, and includes wingtip winglet, twist, or camber morphing. The aerodynamic benefits of these geometry changes include increased lift, enhanced aerodynamic efficiency, and increased control authority^{2,3}. The ability to cause these changes quickly and seamlessly can allow one aircraft to achieve different flight characteristics depending on immediate need.

¹ Student, Mechanical Engineering, AIAA Student Member.

² Assistant Professor, Mechanical Engineering, AIAA Professional Member.

Twist morphing is a type of out-of-plane morphing which allows for change in the wing angle of attack (AOA) without a change in the wing camber. This change in AOA causes wing twist morphing to function much the same as a wing aileron, without the discontinuity of typical discrete ailerons which increases the wing's induced drag¹⁰. A morphing wing with positive twist AOA increases drag due to the larger perpendicular surface, but considerably increases lift^{10,11}. Rodrigue *et al.* proposed an innovative twist morphing method which reduces drag by isolating the twisting actuation to a single portion of the wing¹⁰. The increased lift generated by twist morphing can propagate to enhanced roll control when twisted wings are activated individually or antagonistically.

Camber morphing is an out-of-plane transformation that bends the camber line of the airfoil. This method of morphing utilizes the aerodynamic behavior seen in conventional control surfaces for increasing or decreasing lift potential, without the penalty of large drag profiles associated with surface gaps and discontinuities. Camber morphing techniques are a popular path of research and many designs have been proposed¹²⁻¹⁶. Recently, Bishay *et al*¹⁷ used the "FishBAC" design to camber-morph a UAV tail section. The concept of the Fish Bone Active Camber (FishBAC) morphing airfoil was developed by Woods and Friswell in 2012¹⁸.

This paper introduces a new unmanned aerial vehicle (UAV) with full-morphing capabilities called "Matamorph-2" or XM-2. This new UAV utilizes twist-morphing wings and camber-morphing tail stabilizers. Twist-morphing wings rotate the wing airfoil ribs around the wings central spar. Only one third of the wing undergo the actual twisting motion. This section features low density foam with thin balsa wood ribs to maintain the airfoil shape while allowing the flexible deformation needed for twist morphing. XM-2 empennage utilizes the entire length of the horizontal and vertical stabilizers for morphing. This lightweight design can deform the camber line of the symmetric airfoil to replicate elevators and rudders without any discontinuities.

The rest of this paper is organized as follows: section II presents the preliminary design and sizing approach including some newly developed computer applications that guide the design process. Section III describes all subsystems of XM-2, namely the wings, empennage, fuselage and propulsion and avionics systems. Section VI addresses the CFD and FEA simulations performed. Section V covers actuation testing. Conclusions are summarized in section VI.

II. Preliminary Design and Sizing

The main goal of this work is to design a UAV that has twist-morphing wings and camber-morphing horizontal and vertical tail stabilizers; a UAV that can complete a flight mission without the use of any discrete control surfaces, such as ailerons, elevators and rudders. For simplicity, rectangular planforms were selected for the wing and tail stabilizers. The standard sea level (SSL) conditions (air density $\rho = 1.225 \text{ Kg/m}^3$, air pressure $P = 101.3 \text{ kPa}$, air temperature 15°C) was also assumed during design since the expected flight altitude for UAV is very low. The airplane weight is one of the most important parameters that affect the design. After coming up with the main concepts for morphing the wings and tail stabilizers, a spreadsheet was created and continuously updated to calculate the overall weight of the UAV based on the weights of all components that are to be on the plane including structural components, engine, electronics and control system, etc. In order to make a decision on the span and chord length of the wing, a computer application (App) called "Twisting Wing Analyzer" was developed on MATLAB as shown in Fig. 1. The App needs some general inputs such as the estimated weight of the UAV without wings, the maximum speed, Oswald efficiency factor, air density, and AOA, in addition to ranges for wingspan and wing aspect ratio sweep analysis. The app also requires some inputs related to the specific wing design of XM-2, to be detailed in the following sections, such as the number of ribs, number of spars, foam density, rib material density, number of composite plies, etc. Once the user clicks run, a sweep analysis is performed and the App displays graphs showing the effects of wingspan and wing aspect ratio (or alternatively wing chord length), on the net lift force (overall UAV weight subtracted from the overall lift force) as shown in Fig. 2. According to the sweep study, a wingspan of 3.05 m and an aspect ratio of 6.78 was chosen for the wings in order to minimize induced drag, maximize maneuverability, and ensure sufficient structural integrity could be achieved. This resulted in a chord length of 0.45 m, and wing area of 1.373 m^2 , which would be sufficient to lift the expected weight of the UAV at the speeds the selected motor could handle.

A typical design cruise speed for UAV of 12 m/s (32 mph) was selected. The takeoff speed of the plane was calculated to be 1.2 times the stall speed and using the equation of ground run distance¹⁹, it was found that liftoff rotation will occur at 31.33 m given the amount of speed and lift force that the UAV will experience. The distance needed to clear a 10.67 m (35 ft) obstacle after rotation was found to be 18.3 m, with a 30° climb angle. This results in a total takeoff length of 49.63. An AOA of 10 degrees of twist was used to perform these calculations. The landing approach speed was calculated to be 1.3 times the stall speed, where a speed of 1.1 times the stall speed needs to be achieved when flaring for touchdown to avoid any premature stalling of the UAV. The landing distance was calculated using the same takeoff equation but thrust and lift were removed. The drag of the aircraft combined with the friction

between the wheels of the landing gear and the runway are the only forces actively slowing the UAV after touching down. The landing distance at maximum AOA was found to be 145.8 m using the aforementioned parameters.

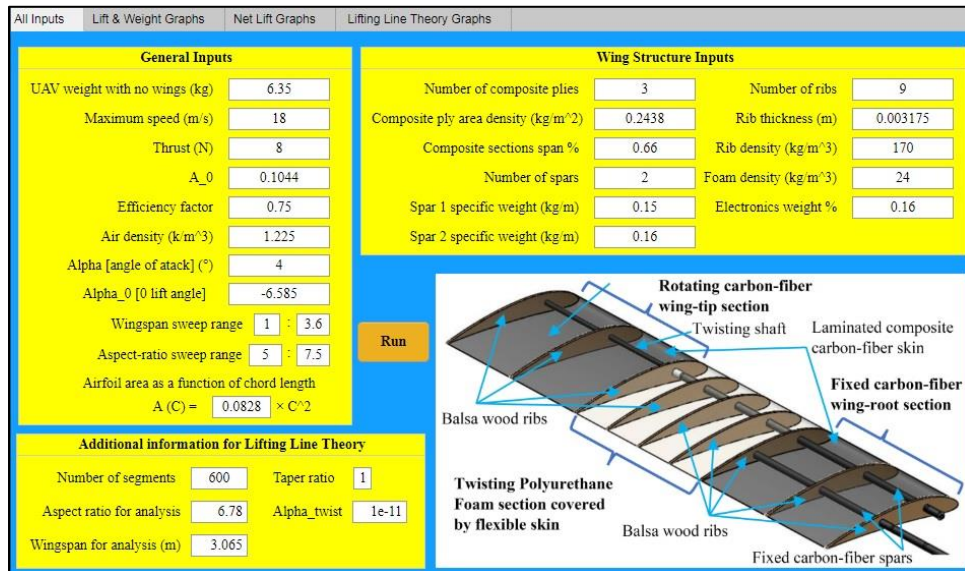


Fig. 1 “Twisting Wing Analyzer” App for wing design

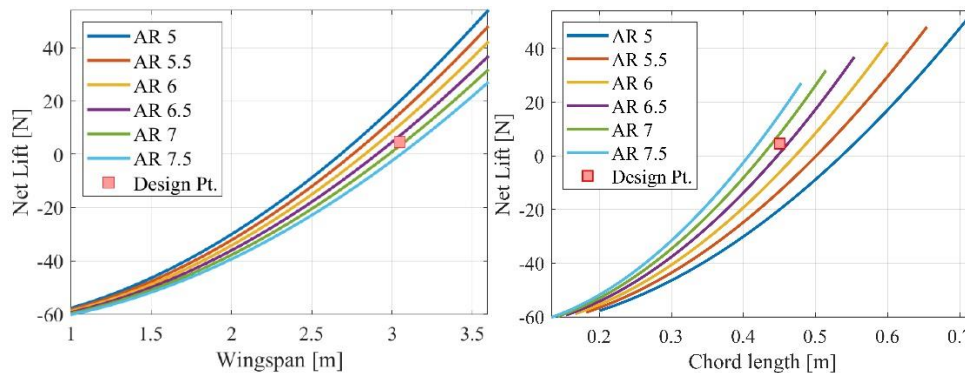


Fig. 2 Calculated net lift force vs. wingspan and chord length

To determine the dimensional parameters for the horizontal and vertical stabilizers, another App, called “Tail Sizing,” was created on MATLAB, as shown in Fig. 3.

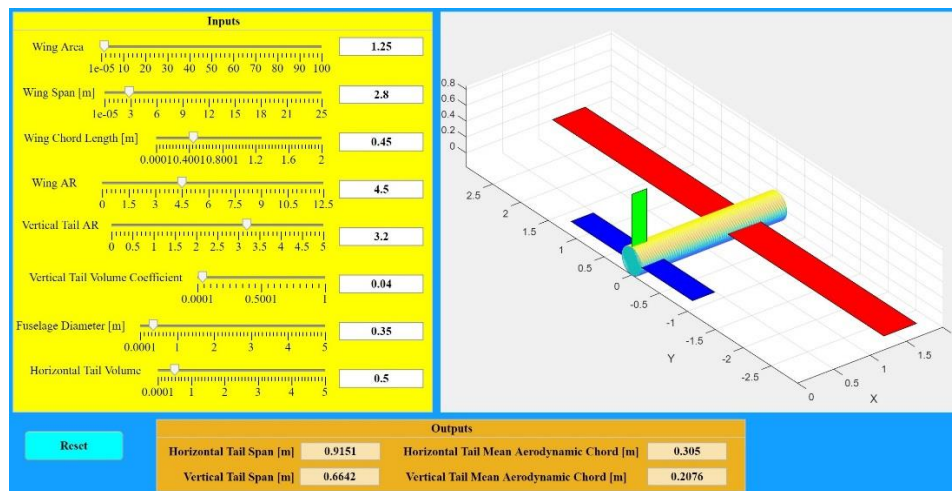


Fig. 3 “Tail Sizing” App

The app uses inputs such as wing area, wing aspect ratio (or alternatively wingspan and chord length), fuselage diameter, vertical tail aspect ratio and volume coefficient to create a schematic of the plane as shown in the figure and calculate the span and chord of the vertical and horizontal stabilizers, following the design approach in Sadreay's aircraft design textbook²⁴. The App has sliders to dynamically change any of the input parameters and immediately see the resulting airplane shape and tail geometric parameters.

III. Model Description

Fig. 4 shows the full assembly of XM-2. The fuselage houses the motor in the nose cone, servomotors that actuate the wings, and all electronic components. The main landing gear is fixed to the bottom of the fuselage. Each wing is made of fixed wing-root section, twisting section and a rotating wing section. The tail boom connects the fuselage to the camber-morphing vertical and horizontal tail stabilizers. The length of the plane is 2.21 m.

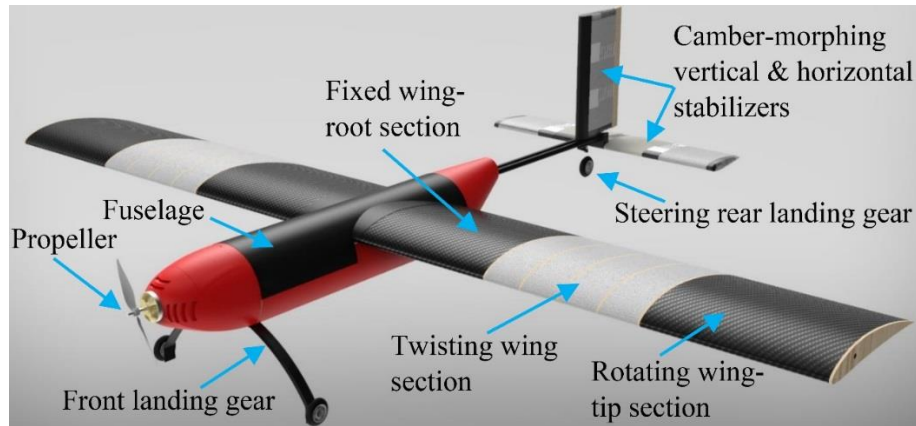


Fig. 4 XM-2 assembly

A. Wing Design

Fig. 5 Shows the CAD assembly of the wing structure. The span of each of the three wing sections is one-third the span of the whole wing. NACA 6412 airfoil was chosen for XM-2's wings based on ease of manufacturability, low drag and high lift profiles. All ribs in the three sections of the wing are made of Balsa wood, which has a high stiffness-to-weight ratio. The fixed wing-root and rotating wing-tip sections are made of laminated composite shell structures of three interwoven carbon fiber plies in epoxy matrix. This structure provides a smooth surface as well as sufficient stiffness to carry the aerodynamic loads while maintaining low overall weight. The fixed wing-root section is connected to the fuselage.

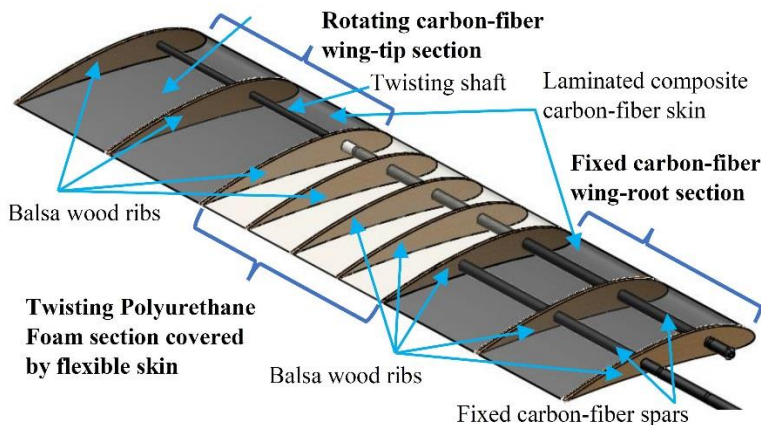


Fig. 5 XM-2 twist-morphing wing

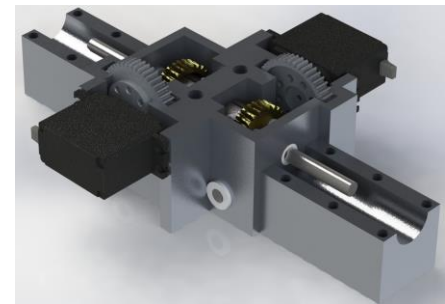


Fig. 6 Wing gearbox

The twisting section is made of four polyurethane foam subsections separated by Balsa wood ribs for reinforcement. These foam subsections take the profile shape of the airfoil and allow the twisting deformation to transition smoothly across the twisting section. The foam subsections are bonded to the wood ribs and the whole twisting section is bonded to the other two composite sections. The twisting section is covered by a polyvinylidene

chloride flexible skin (Saran wrap) with a PVA glue (mod podge) coating. The skin protects the foam from harmful environmental factors, such as moisture in the air that can increase the rate of degradation of the foam, and prevents air from flowing through the porous material. The skin is able to twist with the foam. Two carbon fiber spars run through the fixed wing-root section, but only the main/ front spar runs through the twisting section. A shaft that runs through the rotating wing-tip section feeds through the main spar to enable the twisting deformation. The shaft is connected to a motor gearbox mechanism (shown in Fig. 6) in the fuselage that rotates the twisting section. When actuated, the wing structure deforms smoothly without any discontinuities. The front and rear spars are located at 25% and 60% chord length from the leading edge, respectively. The weights of the three sections are as follows: 0.41 Kg for the fixed wing-root section, 0.38 Kg for the twisting section, and 0.43 Kg for the rotating wing-tip section. Accordingly, keeping the twisting deformation localized in only the middle section, rather than the whole wing, ensures a stiffer wing structure, and avoid potential flutter problems that highly flexible wings experience.

The gearbox that the shaft is connected to in the fuselage has a 9:1 gear ratio to provide nine times the amount of torque that is supplied by the servomotor while also serving as a locking mechanism for the wing deformation. Despite the reduction in actuation speed resulting from the gearbox, the response time is adequate for aircraft maneuverability. Calculations on the expected turn radius of the UAV were performed at various bank angles to determine how much lift is needed, and the turn radii were found for various bank angles at varying speeds. It was found that to perform a turn with a 30° bank angle, a required speed of 16 m/s resulted in a radius of 37.338 m. This turn performance was acceptable considering the large area around the airfield.

B. Empennage

XM-2 empennage possesses an aft positioned tail in a conventional or T-inverted configuration. The horizontal tail is positional aft of the fuselage boom and the vertical tail is on the top aft of the fuselage boom as shown in Fig. 7 (left). Instead of conventional elevators and rudders that provide trim and stability for the aircraft, XM-2 features camber-morphing tail surfaces. The design of the horizontal and vertical stabilizers is very similar. NACA 0015 airfoil was used in both of them. Each stabilizer has a rigid 3D printed Polylactic Acid (PLA) leading-edge section whole length is 40% the chord length. The leading segment allows for the insertion of two carbon fiber spars for rigidity and stiffness. Two active ribs are placed 25% of the span length from the two ends. Two 3D printed flexible Thermoplastic Polyurethane (TPU) inactive ribs are placed at the ends of each stabilizer. Only the horizontal stabilizer has an additional central inactive rib. Polyurethane foam sections that have the same airfoil shape are placed between the ribs as shown in the figure. The active rib, demonstrated in Fig. 7 (right), has an actuation compartment that houses the camber-morphing mechanism and a corrugated section. This is a modified version of the camber-morphing FishBAC design developed by Bishay *et al.*¹⁷ that featured shape memory alloy (SMA) wire actuators. The rib is 3D printed of Plasticized Copolyamide Thermoplastic Elastomer (PCTPE), which has a moderate stiffness that allows for deformation but still provides rigidity to carry the aerodynamic loads in flight. The corrugated section has vertebra-like interior structure that prevents buckling of the outer corrugated shell and maintains the shape of the airfoil. The actuation compartment contains 3D printed threads enabling the mounting of a Hexfly Digital 180-degree servomotor with a 25 kg.cm rated torque along the side of each active rib. Using a servomechanism coupler, two aluminum half-round rods are aligned into the housing and a receiving cap provides translational restraint on the opposite end of the rib. Carbitex CX6 ribbons run from the actuation compartment through rectangular cutouts in the corrugated external shell. CX6 ribbons are fixed between the two aluminum half round rods inside the actuation compartment, and bonded to the corrugated section trailing edge. CX6 is a carbon fiber reinforced flexible thermoplastic material, developed by Carbitex, Inc²⁰, that provides excellent in-plane strength. Rotating the servomotor pulls the ribbon from either side, causing the camber-morphing actuation to happen.

Camber morphing causes a change in the surface area of the wing skin. Hence, a skin that features high strain capability, high strain recovery rate, and relatively high stiff in the spanwise direction to withstand aerodynamic and inertial loads, is required²¹. Neoprene rubber was selected as the skin that covers both horizontal and vertical stabilizers of XM-2. This is a commercial grade 40A flexible rubber sheet that has a smooth surface finish to ensure low friction when introduced to aerodynamic airflow. Because camber morphing is happening in two directions, the top and bottom portions of the skin will experience tension or compression. To ensure smooth surface without buckling under compression, the skin is pre-tensioned when applied.

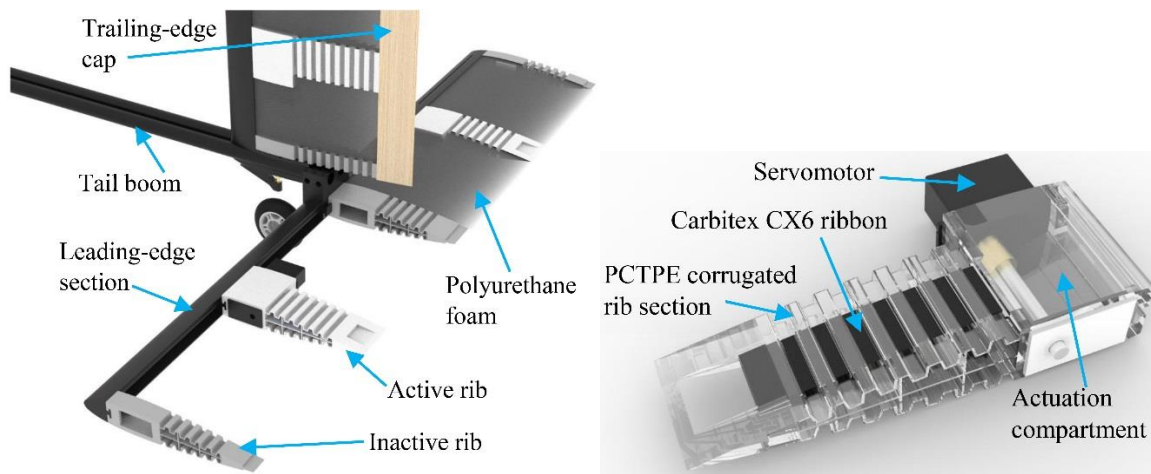


Fig. 7 (Left) XM-2 empennage, (right) XM-2 camber-morphing active rib

C. Fuselage Design

XM-2 features a traditional cone cylinder fuselage that consists of carbon fiber and aluminum as the main structure with a flat bottom cross-section to accommodate a simple and solid integration of the front landing gear. It utilizes a modified tail dragger landing gear layout with two wheels in the front and a swiveling wheel in the rear to enable ground steering with provided input from the empennage vertical stabilizer. The wing mounts onto a 6061-aluminum sheet metal riveted to perpendicular aluminum bulkheads. Two carbon fiber tubes are fixed to the aluminum bulkhead behind the wing and another identical bulkhead at the rear of the fuselage. This structure provides the rigidity and stability needed to mount the empennage in the required position. Sectional carbon fiber tubes connect each bulkhead in the fuselage to increase overall rigidity. Additional rigidity is provided by six pultruded unidirectional carbon-fiber stringers. These stringers, in conjunction with lightweight balsa wood bulkheads, provide support for the aircraft fabric applied as the outer fuselage skin. The motor and avionics system mounts in a 3D printed PLA nose cone with a hollow lightweight 3D printed tail cone. A lightweight removeable cover is mounted on top to allow easy access to the internal components. Fig. 8 shows the internal structure with the aircraft skin and nose cone hidden.

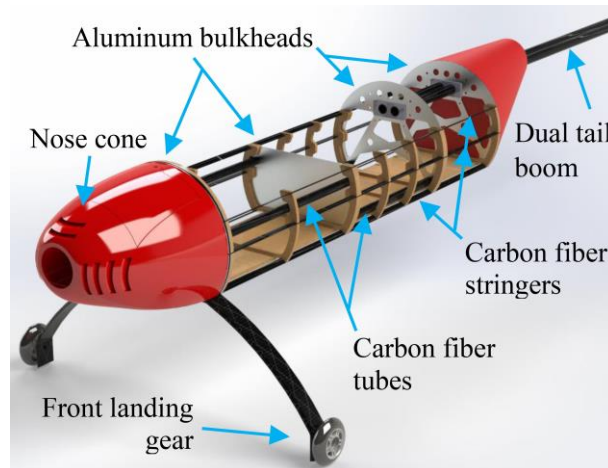


Fig. 8 Fuselage internal structure

XM-2 follows conventional aircraft design for center of gravity (CG) location $1/4$ chord length behind the leading edge of the wing. The fuselage established this CG location with a solid nose cone and minimal material behind the wing.

D. Propulsion and Avionic Systems

The propulsion system selected for XM-2 is a propeller driven system consisting of an electric brushless motor with a composite electric propeller of size $43.2 \text{ cm} \times 20.3 \text{ cm}$. Standard sizing is set by propeller manufacturers

as diameter \times pitch. Motor-induced P-factor is the tendency for the propeller to pull the UAV toward the direction in which the propeller is rotating. This effect was addressed by offsetting the motor 1.5° when mounted to the fuselage of XM-2. The motor selected for XM-2 was the Great Planes Rimfire 1.20 with a Kv rating of 450 as stated by the manufacturer. From this parameter, the motor's RPM can be calculated by multiplying Kv by the applied electric potential. The max theoretical static thrust was found to be 73 N. To compare this with the actual thrust produced by the motor, a test apparatus was designed and manufactured as shown in Fig. 9. Multiple propellers were tested. The actual static thrust measured by the test apparatus was found to be 67 N for the 43.2 cm \times 20.3 cm propeller. This yielded, 8280 RPM, an amp draw of 83A and produced a max burst power of 1712 W, which is within the standard safety limits.



Fig. 9 Apparatus for testing XM-2 motor thrust

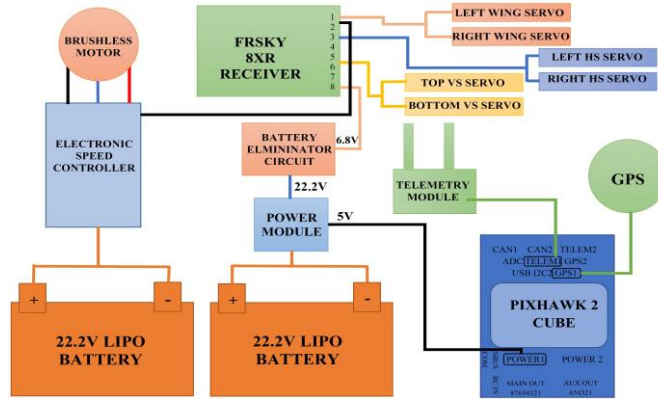


Fig. 10 Wiring diagram showing the electrical components within XM-2

The avionics system in XM-2 consists of the following components: a transmitter, receiver, brushless electronic speed controller (ESC), two 22.2V 5000 mAh lithium polymer (LiPo) batteries, battery eliminator circuit (BEC), six 25kg-cm 180° high torque servos, and the Rimfire brushless motor. A microcontroller (Pixhawk 2.1) is implemented to track and receive data during flight. This device is used to communicate with the ArduPilot ground control software to present information such as altitude, heading, pitch, roll, and coordinate position. The control systems are initiated by the pilot using the transmitter (Taranis QX7). The transmitter outputs a pulse width modulation (PWM) signal to the corresponding output channel in the receiver (FrSky X8R). The signal coming from the receiver is then directly distributed to the motor and actuating servomotors. There are two symmetric high torque servomotors in both the vertical and horizontal stabilizers to actuate the tail. These servomotors use two output channels in the receiver, one for each stabilizer. The total weight of the electrical components in XM-2 sums up to approximately 2.69 Kg. Fig. 10 shows the wiring diagram for XM-2. The propulsion and avionics systems are powered by two individual 22.2 V 5000mAh LiPo batteries. The propulsion system receives power directly from one battery in order to eliminate fluctuating voltage to the controls system. The controls system receives its power through the secondary battery connected to a BEC which steps down the voltage from 22.2 V to 6.8 V. This ensures that a maximum torque is applied to the servomotors. The Pixhawk is powered through a step down from a 5V power module. To avoid back feeding power into the receiver, only the signal and ground of the ESC are connected to the motor.

IV. Analysis and Simulation

A. Modeling Cambered Airfoil

When the tail stabilizers camber-morph, the shape of the airfoil obviously change. In order to model the cambered airfoil, the active rib segment was first bent to several angles, and the mean camber line for each angle was traced. The drawing was then photographed, and the parametric equations of the airfoil at different angles were generated using a graph digitizer. The data was curve-fitted as a second-order polynomial in eq. (1), x represents the horizontal position along the chord starting from the leading edge while c_n is the distance from the leading edge at which the camber deformation begins.

$$y_c(x) = A(x/c)^2 + B(x/c); \quad x \geq c_n \quad (1)$$

where x represents the position along the chord measured from the leading edge, c is the chord length, $c_n = 0.297c$ and A and B are the parameters that control the amount of deformation of the airfoil. The values of A and B are dependent

on the camber angle, and determine the amount of deformation/camber on the airfoil. The NACA parametric airfoil equation is

$$y_t(x) = 5t \left[a_0 \sqrt{x/c} + a_1(x/c) + a_2(x/c)^2 + a_3(x/c)^3 + a_4(x/c)^4 \right], \quad (2)$$

where $a_0 = 0.2969$, $a_1 = -0.126$, $a_2 = -0.3516$, $a_3 = 0.2843$, $a_4 = -0.1036$, and t is the maximum thickness as a fraction of the chord ($t = 0.15$ for NACA 0015 airfoil). So, in order to create the geometry of the airfoil in any CAD or CFD program, the following equation is used

$$y(x) = \begin{cases} \pm y_t(x) & x < c_n \\ \pm y_t(x) + y_c(x) & x \geq c_n \end{cases}. \quad (3)$$

To study the effect of A and B on the deformation of the airfoil, another MATLAB App was created as shown in Fig. 11. The app has sliders to dynamically change A and B values and immediately see the resulting shape.

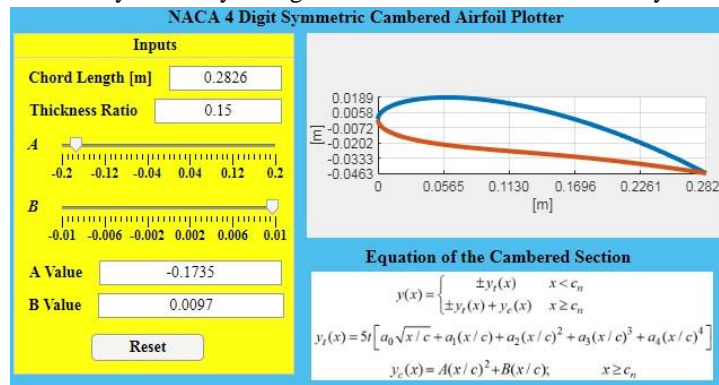


Fig. 11 “NACA 4-Digit Symmetric Cambered Airfoil Plotter” App

B. Computational Fluid Dynamics

Multiple 2D and 3D computational fluid dynamics (CFD) simulations were performed using ANSYS Fluent software to analyze the twisted wings and cambered stabilizers in flight. First, lift and drag coefficients were calculated from 2D simulations on NACA 6412 airfoil at 2.92 m/s and Reynolds number (Re) of 200000. Spalart Alamaras mathematical model was used, and the resulting lift and drag coefficients were equivalent to the values reported in Airfoil Tools²². 3D flow simulations were then conducted on the wing with 0° and 10° twist angle. The k- ω SST mathematical model was used with a velocity of 12 m/s and Re of 350000 yielding a lift force of 50 N at a 10° angle of twist, while at 0° the lift force was 15.5 N. The simulations also confirmed the concept that having a continuous wing surface would improve the overall aircraft efficiency.

A 2D simulation was also performed on NACA0015 airfoil using ANSYS Fluent to investigate the effect of changing the camber angle at a speed of 12 m/s. Fig. 12 shows the CFD domain and mesh details. Since the chord length, C , is 0.2826 m, R was taken as 15 m, and D as 25 m to eliminate the wall effect. Unstructured mesh that includes both triangular and quadrilateral elements was used with local mesh refinement around the airfoil. Unstructured mesh converged more efficiently, compared to structured mesh that has only quadrilateral elements, specially when modeling cambered airfoils at high angles of attack. The mesh around the airfoil surface is made of very thin layers of elements to account for the turbulent boundary layers (the overlap layer, the buffer layer, and the viscous sublayer). The flow is laminar but becomes turbulent as we go away from the airfoil surface. Due to the low Re and Mach number, the air is assumed incompressible. Spalart Allmaras turbulence model was used because it demonstrated a more desirable convergence than k- ω SST turbulent model for low Re. Fig. 14 shows the effect of camber angle on c_l / c_d ratio. A maximum c_l / c_d ratio of 42.03 was obtained when the camber angle is 8°. The maximum c_l value of 1.76 occurs at 14° camber angle, but the drag significantly increases past the 8° camber angle. A comparison was made between airfoils of different configurations as shown in Fig. 13: (A) 8° cambered airfoil, (B) airfoil with a plain flap, (C) airfoil with slat and plain flap, (D) airfoil with slotted flap, and (E) airfoil with slat and slotted flap. The 8° cambered airfoil is the most efficient configuration at low angles of attack as shown in Fig. 15. The second best at low AOA's is the plain flap configuration with maximum c_l / c_d ratio of 35.55. This dramatic increase in the aerodynamic efficiency at low angles of attack confirms the superiority of seamless camber-morphing designs.

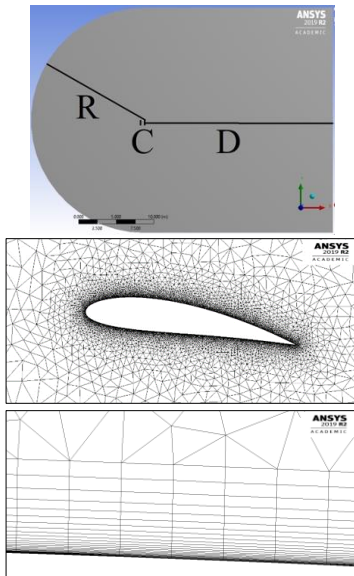


Fig. 12 CFD mesh details

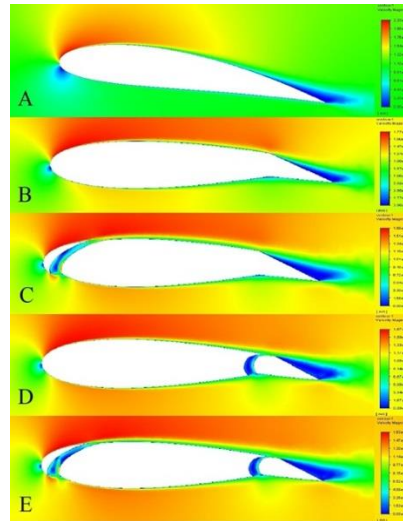


Fig. 13 Velocity contours around different airfoil configurations

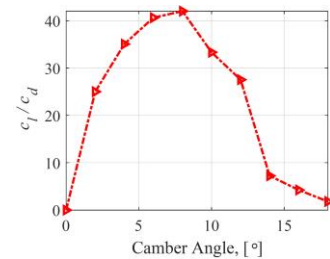


Fig. 14 c_l / c_d vs. camber angle

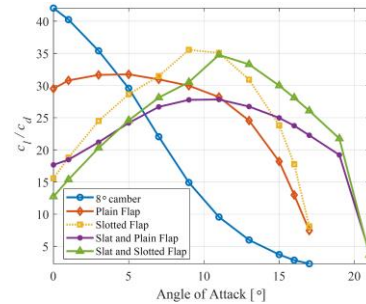


Fig. 15: c_l / c_d comparison

C. FEA Analysis

After completing all CFD simulations, the aerodynamic pressure distribution data were used to run finite element analysis (FEA) on various components of the wings. Fixed boundary conditions were applied to the portions of the structure that are mounted to the fuselage. A 51 N distributed load was applied across the spar structure of the wing and a 15.4 N distributed load across the twisting shaft, yielding a maximum displacement of 23.4 mm at the extreme end of the rotating shaft. The fixed carbon-fiber wing section including the ribs was also analyzed with a 14.3 N lift force and 1.1 N drag force as shown in Fig. 16. The maximum displacement was found to be 0.4 mm. The maximum local stress along the composite thickness was far from the ultimate stress and Tsai-Hill failure criterion for composites proved the structure is safe. Hence, the expected aerodynamic loads would not damage the structure or cause any severe deformations past the point of functionality.

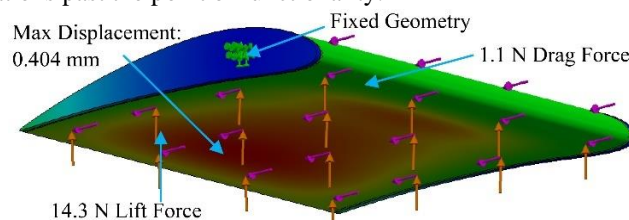


Fig. 16 FEA Analysis of the carbon-fiber wing-root fixed section

V. Testing

Mechanical testing was done first on different components and subsystems. For example, the tail active rib was tested with some weights attached to its trailing edge to simulate expected aerodynamic loads. The servomotor was able to generate the required torque and the rib deformed as expected. Fig. 17 shows a camber morphing of 15° with 700 gm attached. This demonstrates the integrity of the chosen servomotor, and the ability of the rib structure to undergo the required morphing without failure. Fig. 18 shows the manufactured horizontal stabilizer before applying the flexible skin.



Fig. 17 Active rib morphing with 700 gm weight

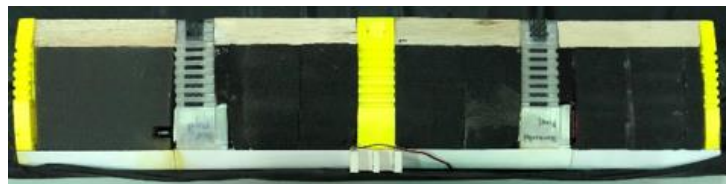


Fig. 18 Assembled horizontal structure without skin

Fig. 19 shows the assembled and actuated twist-morphing wing to 16° twist angle. Fig. 20 shows the horizontal and vertical camber-morphing stabilizers with the flexible skin actuated to 9° and 8° respectively. Finally, Fig. 21 shows the full assembly of the manufactured model of XM-2.



Fig. 19 Wing twist actuation



Fig. 20 Horizontal (left) and Vertical (right) stabilizers camber actuation



Fig. 21 XM-2 assembled

VI. Summary and Conclusion

Morphing wing designs have been developed but were rarely implemented in full-scale models. This paper introduced XM-2 as a fully morphing UAV with seamless twist-morphing wings and camber-morphing tail stabilizers. XM-2 has no conventional discrete control surfaces. A traditional fuselage design was utilized to simplify the integration of the wing and tail stabilizers. The wing is partitioned into two stiff hollow carbon-fiber sections that sandwich a third twisting reinforced foam section. The internal structure is supported by carbon fiber spars that enable twisting the wing $\pm 15^\circ$ utilizing servo-gearbox subassembly mounted in the fuselage. The horizontal and vertical stabilizers are composed of PCTPE active ribs, TPU inactive supporting ribs, PLA leading edge caps and mounts, low density polyurethane foam and balsa wood trailing edges supported by a combination of carbon fiber and basswood spars. The core is covered by wrapping it with elastic Neoprene skin. Camber morphing of 8° allows for maximum C_L/C_D . In-house MATLAB applications were developed to help in the design phase. CFD and FEA simulations were done to confirm the design decisions. Actuation and mechanical testing were done on different components and subsystems. The whole plane was manufactured and assembled. Flight tests would be conducted to demonstrate the capabilities of XM-2 in real life.

VII. ACKNOWLEDGEMENT

This work was done by the fourth cohort of “Smart Morphing Wing” research-based senior design project (SDP) at California State University, Northridge (CSUN). The following members are acknowledged: Artur Balyan, Jake Alger, Mathan Vasu, Marcelo Carlos Rodel, Antony Khalil, Rafael Reyes, Leonardo Flores, and Rommel Herrera. The authors acknowledge the Mechanical Engineering Department, the Instructionally-Related Activities (IRA) grant, and the Associated Students-Student Travel and Academic Research (AS-STAR) grant at CSUN. CSUN Human Powered Vehicle (HPV) and CSUN Aeronautics SDP’s are acknowledged for their support throughout the lifespan of the project. Carbitex Inc. is also acknowledged for their generous donations.

References

- ¹ Sun, J., Guan, Q., Liu, Y., and Leng, J., “Morphing Aircraft Based on Smart Materials and Structures: A State-of-the-art Review,” *Intelligent Material Systems and Structures*, vol. 27, no. 17, 2016, pp. 2289-2312. doi: doi.org/10.1177/1045389X16629569
- ² Sofla, A.Y.N., Meguid, S.A., Tan, K.T., and Yeo, W.K., “Shape Morphing of Aircraft Wing: Status and Challenges,” *Materials and Design*, vol. 31, 2010, pp. 1284-1292. doi: 10.1016/j.matdes.2009.09.011
- ³ Joshi, S.P., Tidwell, Z., Crossley, W.A., and Ramakrishnan, S., “Comparison of Morphing Wing Strategies Based Upon Aircraft Performance Impacts,” *AIAA Structures Dynamics & Materials Conference*, Palm Springs, CA, 2004. doi: 10.2514/6.2004-1722
- ⁴ Min, Z., Khac, V., and Richard, L.J.Y., “Aircraft Morphing Wing Concepts with Radical Geometry Change,” *The IES Journal Part A: Civil & Structural Engineering*, vol. 3, no. 3, 2010, pp. 188-195. doi: 10.1080/19373261003607972
- ⁵ Ajaj, R.M., Beaverstock, C.S., and Friswell, M.I., “Morphing Aircraft: The Need for a New Design Philosophy,” *Aerospace Science and Technology*, vol. 49, 2016, pp. 154-166. doi: doi.org/10.1016/j.ast.2015.11.039
- ⁶ Gomez, J.C., and Garcia, E., “Morphing Unmanned Aerial Vehicles,” *Smart Materials and Structures*, vol. 20, 2011. doi: 10.1088/0964-1726/20/10/103001
- ⁷ Benjamin, J., Calisch, S., Cellucci, D., Cramer, N., Gershenfeld, N., Swei S., and Cheung, K.C. “Digital Morphing Wing: Active Wing Shaping Concept Using Composite Lattice-Based Cellular Structures”, *Soft Robotics*, vol 4, no. 1, 2017, doi: 10.1089/soro.2016.003233
- ⁸ Ajaj, R.A., Jankee, G.K., “The Transformer Aircraft: A Multimission Unmanned Aerial Vehicle Capable of Symmetric and Asymmetric Span Morphing”, *Aerospace Science and Technology*, vol. 76, 2018, pp. 512-522, doi: 10.1016/j.ast.2018.02.022
- ⁹ Chanzy, Q., Keane, A.J., “Analysis and experimental validation of morphing UAV wings”, *The Aeronautical Journal*, vol. 122, No. 1249, March 2018, pp 390–408, doi:10.1017/aer.2017.130
- ¹⁰ Rodrigue, H., Cho, S., Han, M., Bhandari, B., Shim, J., and Ahn, S., “Effect of Twist Morphing Wing Segment on Aerodynamic Performance of UAV,” *Journal of Mechanical Science and Technology*, vol. 30, no. 1, 2016, pp. 229-236, doi: 10.1007/s12206-015-1226-3
- ¹¹ Ismail, N.I., Zulkifli, A.H., Abdullah, M.Z., Basri, M.H., and Abdullah, N.S., “Optimization of Aerodynamic Efficiency for Twist Morphing MAV wing,” *Chinese Journal of Aeronautics*, vol. 27, no. 3, 2014, pp. 475-487, doi: 10.1016/j.cja.2014.04.017
- ¹² Markandeyulu, T., Naganna, T., and Muppalla, D., “Design and Analysis on Flex foil of Wing”, *International Journal of Novel Research in Electrical and Mechanical Engineering*, vol. 2, no. 3, pp. 146-153. doi:12/2015 ISSN 2394-9678
- ¹³ Monner, H.P., Hanselka, H. and Breitbach, E., “Development and design of flexible Fowler flaps for an adaptive wing,” *Proc. SPIE Smart Structures and Materials*, vol. 3326, 1998, pp. 60–70. doi: 10.1117/12.310673
- ¹⁴ Campanile, L.F. and Sachau, D., “The Belt-Rib Concept: A Structronic Approach to Variable Camber,” *Journal of Intelligent Material Systems and Structures*, vol. 11, 2000, pp. 215–224. doi: 10.1106/6H4B-HBW3-VDJ8-NB8A.
- ¹⁵ Kota, S., Hetrick, J.A., Osborn, R., Paul, D., Pendleton, E., Flick, P. and Tilmann, C., “Design and Application of Compliant Mechanisms for Morphing Aircraft Structures,” *Proc. SPIE Smart Structures and Materials*, vol. 5054, 2003, pp. 24–33. doi: 10.1177/104538903035563
- ¹⁶ Meguid, A., Su, Y. and Wang, Y., “Complete Morphing Wing Design Using Flexible-Rib System,” *International Journal of Mechanics and Materials in Design*, vol. 13, no. 1, 2015, pp. 159-171. doi: 10.1007/s10999-015-9323-0.
- ¹⁷ Bishay, P.L., Finden, R., Aslanpour, D., Lopez, E., Alas, C., Recinos, S., Flores, D., Gonzalez, E. and Popa, R., “Development of an SMA-Based Camber Morphing UAV Tail Core Design,” *Smart Materials and Structures*, vol 28, no. 7, 2019, doi:10.1088/1361-665X/ab1143
- ¹⁸ Woods, B.K.S. and Friswell, M.I., “Preliminary Investigation of a Fishbone Active Camber Concept,” *Proceedings of ASME SMASIS*, 2012, pp. 555–563. doi:10.1115/SMASIS2012-8058
- ¹⁹ Sadraey, M.H. *Aircraft Design - A Systems Engineering Approach*. Wiley, 2013.
- ²⁰ Flexible carbon fiber: Carbitex CX6, <https://www.carbitex.com/cx6>
- ²¹ Kikuta, M.T. *Mechanical properties of candidate materials for morphing wings*, 2003, Department of Mechanical Engineering, Virginia Polytechnic Institute and State University.
- ²² Airfoil Tools (n.d.), <http://www.airfoiltools.com>